Self-similar hierarchies and attached eddies

Beverley J. McKeon

Phys. Rev. Fluids **4**, 082601 — Published 26 August 2019

DOI: 10.1103/PhysRevFluids.4.082601

Self-similar hierarchies and attached eddies

Beverley J. McKeon[1,*]

[1] *Graduate Aerospace Laboratories, California Institute of Technology, Pasadena, California 91125, USA*

(Dated: August 12, 2019)

It is demonstrated that time-evolving coherent structures with features consistent with Townsend's attached eddies and the developments associated with the reconstruction of flow statistics using the attached eddy hypothesis can be obtained from analysis of the (linear) resolvent operator associated with the Navier-Stokes equations. A discrete number of members of a single self-similar hierarchy, chosen by assuming a constant ratio of critical layer heights between neighboring members with overlapping wall-normal footprints, produces geometrically self-similar, fractal-like structure of the spatial distribution of the velocity field and an associated signature of uniform momentum zones. The range of convection velocities associated with the hierarchy give rise to time evolution of the velocity. The scaling of the streamwise wavenumber on a hierarchy can be reconciled with Townsend's distance-from-the-wall scaling for self-similar, attached eddies, at least conceptually, by considering coherent spatial structures in the velocity field and thus enforcing an exact equivalence between compared features. It has been shown previously that both the linear and nonlinear terms in the resolvent framework have self-similar representations in the logarithmic overlap region of the turbulent mean velocity profile. The conditions under which self-sustaining self-similar behavior may be obtained from self-similar hierarchical members in this region are elaborated and some similarities with other results and theories associated with self-similarity in this region are identified.

I. SELF-SIMILARITY: STRUCTURAL AND SPECTRAL REPRESENTATIONS

Townsend's [1] seminal distance-from-the-wall scaling has underpinned many theoretical and observational descriptions of wall turbulence. The original argument posits that eddies with diameters proportional to distance from the wall should be required in order to obtain a dissipation length-scale also proportional to this distance in the equilibrium (or inertial) layer, such that the motion of "the main eddies of the flow... is directly influenced by its presence" [2]. He proposed using a self-similar function, s_1, to model the velocity field $\tilde{\mathbf{u}} = (u, v, w)$ for an eddy centered at (x_a, y_a, z_a) and superimposed on a uniform background flow,

$$\tilde{\mathbf{u}}(x, y, z) = s_1 \left[\frac{(x - x_a)}{y_a}, \frac{(y - y_a)}{y_a}, \frac{(z - z_a)}{y_a} \right]. \tag{1}$$

These ideas have been elaborated effectively over several years into the attached eddy model (AEM), most recently reviewed in [3], which deploys a (static, linear) superposition of hierarchies of self-similar eddies and gives rise to a range of scaling results for the statistics of the velocity field which are well borne out in experimental and numerical data, e.g. [4–7], as well as physical interpretation of the flow arrangement in the inertial region, e.g. [8]. In a discrete representation, the wall-normal eddy lengthscales (heights), $\delta_{E,i}$, are related by a geometric progression and the structures are randomly distributed over wall-parallel planes with the number of structures belonging to hierarchy i described by $N_i \sim y_i^{-2}$. Knowledge of the precise self-similar eddy form is not required to recover logarithmic scaling for the mean velocity profile and wall-parallel fluctuation variances and a constant v-variance, but is important for precise matching of higher order statistics. Recent work [9] has shown that including a spatial exclusion condition to prevent eddies of the same hierarchy overlapping each other leads to improved capture of higher-order statistics. Perry & Marusic [10] noted that a wall-normal extent which scales with distance from the wall can be obtained by two types of eddies: those which reach down to the wall, i.e. $\delta_{E,i} = y_i$, as well as those which do not, $\delta_{E,i} < y_i$, which they denoted as Type-A and Type-B eddies, respectively. The inclusion of Type-B eddies improved the accuracy of the AEM in the wake region of the flow. Information on the eddy dynamics is not immediately available (but could be determined using the Biot-Savart calculations). The predictive capabilities of the attached eddy model are rightly celebrated, and the subject of significant current study.

Flores & Jiménez [11] and Hwang & Bengana [12] have identified self-sustaining turbulent solutions to the Navier-Stokes equations in channel flow simulations with domains restricted to be proportional to distance from the wall, while recent work by Yang *et al.* [13] identifies families of attached exact coherent structures. The statistics of these

* mckeon@caltech.edu

flows are consistent with the properties of attached eddies, and thus appear to provide evidence that the latter are multi-scale and self-sustaining within the minimal unit construction introduced by Jiménez & Moin [14]. Further, these studies give information on the dynamics of such flows, which strongly resemble those of the near-wall cycle identified in the original study. The mean momentum balance analysis (MMB) of Klewicki *et al.* , e.g. [15], identifies self-similar scaling layers contributing to the mean Reynolds stress and therefore the mean velocity profile.

These works provide physical space (structural) proposals for, or identification of, attached eddies, with the numerical studies also documenting their spectral signature. Separate work related to the linear dynamics of the Navier-Stokes equations (NSE) has identified self-similarity of the input-output response. del Alamo & Jiménez [16] noted self-similarity of transient growth modes obtained from analysis of the NSE linearized relative to the turbulent mean velocity profile and Hwang & Cossu [17] observed geometric self-similarity of the most-amplified velocity response to harmonic and stochastic input forcing in the logarithmic region. Both of these studies used an eddy viscosity to provide closure of the equations. Here we exploit the development of McKeon & Sharma [18] in which the terms that are nonlinear in the fluctuations provide the forcing to sustain the linear dynamics, obviating the need to use an eddy viscosity and leading to a closed feedback loop (sketched in, e.g. [19], figure 1). Moarref *et al.* [20–22] have documented the self-similarity of both linear and nonlinear terms in the log region. Self-similar hairpin vortex structures were also observed by Sharma *et al.* [22] using resolvent analysis, while Vadarevu *et al.* [23] observed self-similar, attached structure in the impulse response of the eddy-viscosity-modified linearized Navier-Stokes operator.

The approach is outlined briefly below; the reader is referred to, e.g. [24], for complete details. Consider the equations governing the instantanous motion for a periodic turbulent channel flow under the Reynolds decomposition, $\tilde{\mathbf{u}}(x,y,z,t) = \mathbf{U}(y) + \mathbf{u}(x,y,z,t)$ and $\tilde{p}(x,y,z,t) = P(y) + p(x,y,z,t)$. Denoting the nonlinear term by $\mathbf{f}$, and Fourier transforming in the homogenous spatial directions and in time leads to the equation for a given wavenumber/frequency triplet, $\mathbf{k} = (k_x, k_z, \omega)$, and yields

$$-\mathrm{i}\omega\hat{\mathbf{u}} + (\mathbf{U}\cdot\nabla)\hat{\mathbf{u}} + (\hat{\mathbf{u}}\cdot\nabla)\mathbf{U} + \nabla\hat{p} - (1/Re_\tau)\Delta\hat{\mathbf{u}} = \hat{\mathbf{f}}, \quad \nabla\cdot\hat{\mathbf{u}} = 0, \tag{2}$$

Here $\hat{\cdot}$ denotes a variable in the Fourier-transformed domain, $\nabla = [ik_x, \partial_y, ik_z]$, $\Delta = \partial_{yy} - k^2$, $k^2 = k_x^2 + k_z^2$ and $Re_\tau = hu_\tau/\nu$, where h is the channel half-height, u_τ is the friction velocity and ν the kinematic viscosity. This can be written in terms of the resolvent operator, $H(\boldsymbol{\lambda}, c)$, which can be constructed with knowledge only of the mean velocity profile, where we introduce $\boldsymbol{\lambda} = (\lambda_x = 2\pi/k_x, \lambda_z = 2\pi/k_z)$ for convenience and $c = \omega/k_x$. Here the mean is one-dimensional, $\mathbf{U} = [U(y), 0, 0]$. The resolvent has been shown to be low-rank for $\mathbf{k}$ combinations where wall turbulence is active, e.g. [20], thus a singular value decomposition of this operator using an energy norm can be used to obtain an effective (rank-N) approximation of it, in terms of response and forcing singular modes, $\psi_j(y)$ and $\phi_j(y)$, respectively, where a complex conjugate is denoted by $\cdot^*$:

$$\hat{\mathbf{u}}(y,\boldsymbol{\lambda},c) = H(\boldsymbol{\lambda},c)\,\hat{\mathbf{f}}(y,\boldsymbol{\lambda},c), \qquad H(\boldsymbol{\lambda},c) \approx \sum_{j=1}^{N} \psi_j(y,\boldsymbol{\lambda},c)\sigma_j(\boldsymbol{\lambda},c)\phi_j^*(y,\boldsymbol{\lambda},c). \tag{3}$$

Then the velocity and forcing can be approximated as a weighted sum of resolvent modes,

$$\hat{\mathbf{u}}(y,\boldsymbol{\lambda},c) = \sum_{j=1}^{N} \chi_j(\boldsymbol{\lambda},c)\,\sigma_j(\boldsymbol{\lambda},c)\;\boldsymbol{\psi}_j(y,\boldsymbol{\lambda},c), \tag{4}$$

$$\hat{\mathbf{f}}(y,\boldsymbol{\lambda},c) = \sum_{j=1}^{N} \chi_j(\boldsymbol{\lambda},c)\;\boldsymbol{\phi}_j(y,\boldsymbol{\lambda},c) \tag{5}$$

with the weights, $\chi_j(\boldsymbol{\lambda}, c)$, determined by projecting the true nonlinear forcing onto the forcing modes,

$$\chi_l^*(\boldsymbol{\lambda},c) = \sum_{i,j=1}^{N} \iint \mathcal{N}_{lij}(\boldsymbol{\lambda},c,\boldsymbol{\lambda}',c')\,\chi_i(\boldsymbol{\lambda}',c')\,\chi_j^*(\boldsymbol{\lambda}'',c'')\;\mathrm{d}\ln\boldsymbol{\lambda}'\,\mathrm{d}c', \tag{6}$$

$$\mathcal{N}_{lij}(\boldsymbol{\lambda},c,\boldsymbol{\lambda}',c') = -\sigma_i(\boldsymbol{\lambda}',c')\sigma_j(\boldsymbol{\lambda}'',c'')\int_0^2 \phi_l^*(y,\boldsymbol{\lambda},c)\cdot\left(\psi_i(y,\boldsymbol{\lambda}',c')\cdot\nabla\psi_j(y,\boldsymbol{\lambda}'',c'')\right)\,dy. \tag{7}$$

Here the interaction coefficient, $\mathcal{N}_{lij}(\boldsymbol{\lambda}, c, \boldsymbol{\lambda}', c')$, describes the projection of the forcing arising from the interaction between two response modes at $\boldsymbol{\lambda}', \boldsymbol{\lambda}''$ onto the l-th forcing mode at $(\boldsymbol{\lambda}, c)$.

II. SELF-SIMILAR STRUCTURE ON RESOLVENT HIERARCHIES

Moarref *et al.* [20] identified the conditions for self-similarity of the resolvent and geometric self-similarity of the singular functions and values) to be: logarithmic variation of the mean velocity in a region bound by $y_l^+ \leq y^+ \leq y_u Re_\tau$, localization of the response modes to this log region, and a constraint on the aspect ratio, $k_z/k_x = \gamma \gg 1$. We enforce these conditions and examine the first resolvent modes. Self-similar hierarchies can then be defined as subsets $\mathcal{S}(\boldsymbol{\lambda}_r)$ of all mode parameters $\mathcal{S}$ such that,

$$\mathcal{S}(\boldsymbol{\lambda}_r) = \Bigg\{ (\boldsymbol{\lambda}, c) \,|\, \lambda_x = \lambda_{x,r}\Big(\frac{y_c^+ y_c}{y_r^+ y_r}\Big),\ \lambda_z = \lambda_{z,r}\Big(\frac{y_c}{y_r}\Big),\ c = c_r + \frac{1}{\kappa}\ln\Big(\frac{y_c^+}{y_r^+}\Big), \\ y_c^+ \geq y_{l'}^+ = \max\{y_l^+, \gamma y_u^+(\lambda_{z,u}/\lambda_{x,u})\},\ y_c \leq y_u \Bigg\}. \tag{8}$$

where $\boldsymbol{\lambda}_r$ denotes the wavelengths of an arbitrary reference mode in that hierarchy and $U(y_c) = c$. All modes on a hierarchy are geometrically self-similar [20]. Wall-normal scaling with y_c is a consequence of the localization of the response due to the existence of a critical layer, and is consistent with attached eddy scaling. Similarly, $\lambda_z \sim y_c$, however $\lambda_x \sim y_c^2$ instead of simply y_c for constant Reynolds number, i.e. the self-similarity of the resolvent yields a self-similar hierarchy function s_2 [22], which differs from s_1:

$$\tilde{\mathbf{u}}(x, y, z) = s_2\left[\frac{(x - c\,t)}{y_c y_c^+}, \frac{(y - y_c)}{y_c}, \frac{(z - z_c)}{y_c}\right]. \tag{9}$$

The former pertains to spectral scaling, while the AEM is developed from the spatial distribution of self-similar, coherent physical (low-velocity) structures. Thus the coherent physical structure associated with members of a resolvent hierarchy represents a more faithful point of comparison to attached eddies as proposed by Townsend. Figure 1 shows isosurfaces of the streamwise velocity field associated with five members of hierarchy $\mathcal{S}_{h1}$ with $y_r^+ = 3\sqrt{Re_\tau}$ and $\boldsymbol{\lambda}_r = (29, 123, U(y_r)$, at $Re_\tau = 15,000$, i.e.

$$u(x, y, z, t) = \sum_{m=1}^{5} A^{m/2}\psi_1(y, \boldsymbol{\lambda}_m, c_m)e^{ik_{xm}[x + \gamma_m z - c_m t]}, \tag{10}$$

where A relates the y-locations of the members of the hierarchy through $y_{c,m} = A^{1-m}y_{c,1}$. For this analysis, $|A| = 2$ to ensure overlap in y between the fluctuations associated with consecutive modes, and for consistency with recent implementations of the AEM. For panels (a)-(d) (and (h)), each mode is symmetric about $z = 0$. The lowest member of the hierarchy is centered at the start of inertial scaling of the mean profile, $y_{c,5}^+ = y_r^+ = 3\sqrt{Re_\tau}$ [4] and the highest member is constrained to have $y_{c,1} \leq y_u = 0.4$. The streamwise wavelengths are all in the spectral region in which [5] observed wall scaling via coherence measurements. The mode amplitudes were selected to give the same peak value, which is $0.1U(1)$. The exact values of the composite velocities in Figure 1 are dependent on the choice of magnitudes, however the location of the isosurfaces of zero fluctuation are only weakly so. Each mode convects with a different convection velocity, $c_m = U(y_{c,m})$, such that the relative phases between modes - and therefore the zero isocontour locations - are functions of time. The relative spanwise phase between modes on the hierarchy can be varied without altering the following observations.

The velocity field associated with Equation 10 reflects the self-similarity of the hierarchy in a visually-striking manner. Coherent wall-normal structure, associated with the aggregation of low speed regions arising from the different modes on the hierarchy and delineated by the isocontours of zero fluctuation, can be clearly observed in the streamwise/wall-normal planes in Figure 1(a-d) (also in three dimensions in (e-f)). While the (spatial) frequency of individual members of the hierarchy is dictated by the wavenumber scaling on a hierarchy, the coherent aggregated structures require a different accounting. Two of the largest aggregated regions of negative velocity, with local minima at $y_{c,1} = 0.4$ and footprints which reach down to the lowest $y_{c,m}$ can be observed in Figure 1(a). The increasing "forking" corresponds to encompassing increasing numbers of periods of the lower hierarchy members. Between these two large structures are two centered at the next lowest y_c, i.e. $y_{c,2} = 0.2$, and so on.

Three-dimensional isosurfaces of constant negative instantaneous velocity corresponding to aggregated structures when mode phases are such that each mode is antisymmetric about $z = 0$ (for ease of visualization) are shown in Figure 1(e). Figures 1(f) and (g) show an isosurface in one period of the largest aggregated structure, $[\lambda_{x,1}, \lambda_{z,1}/2]$, with different spatial regions color-coded to correspond to aggregated structures of different spatial scale, i.e. whose dimensions scale with each $y_{c,m}$, with only $m = 1:3$ shown for clarity. As most easily seen from below in Figure 1(g),

the total number of structures of the three scales shown are $N_1 = 1$, $N_2 = 4$ and $N_3 = 16$. The smaller scales also bear out the scaling relationship

$$N_m = \left(\frac{y_{c,m}}{y_{c,1}}\right)^2 N_1. \tag{11}$$

These aggregations (henceforth simply called structures) are attached in the sense of Townsend and the AEM in as much as their wall-normal dimension, or coherence, scales with distance from the wall. The averaged numbers of structures in the streamwise and spanwise directions obey the attached eddy scaling, but with a spatial exclusion which extends to eddies at different levels within the hierarchy, i.e. different $y_{c,m}$, rather than simply for the same $y_{c,m}$ which would be analogous with the proposal of [9]. Equation 9 can be modified to give

$$\tilde{\mathbf{u}}(x,y,z,t) \;=\; s_3\left[\frac{(x-c\,t)}{y_c}, \frac{(y-y_c)}{y_c}, \frac{z}{y_c}\right], \tag{12}$$

subject to the spatial exclusion constraint. We note in passing the similarity of the aggregations to the branching structure obtained for optimal thermal transport of a passive scalar by [25].

The summation of the mean profile and a single resolvent mode has been shown [26] to replicate the recognizable bulge structure in isocontours of instantaneous velocity, commonly noted in experimental and numerical observations, including the asymmetric (in x) ramp and cliff structures which arise collocated with the half-period of negative velocity fluctuation due to the profile of wall-normal shear. Such features can also be observed in the composite fields of Figure 1(h); the exact geometry of the isosurfaces of velocity is dependent on both the hierarchy under consideration and the mode weight relative to the local mean velocity (Figure 1(i)), i.e. $|\hat{u}(y_c)|/U(y_c) = |\hat{u}(y_c)|/c$.

Of note, this development identifies the convection velocity for each member of the structure hierarchy, which increases with increasing distance from the wall, y_c, since $c \approx U(y_c) = 1/\kappa \ln y_c^+ + B$. Thus the images of Figure 1 evolve in time in a simple way. Moving in the frame of the m-th mode on a hierarchy, i.e. convecting downstream at c_m, and considering the relative passing frequencies of the modes immediately above and below on the hierarchy, i.e. $\breve{\omega}_{m\pm1} = k_{x,m\pm1}(c_{m\pm1} - c_m) = \mp A^{\pm2} k_{x,m} y_{c,m}^2 1/\kappa \;\ln A$, it can be shown that $\breve{\omega}_{m+1}/\breve{\omega}_{m-1} = -A^4$. Thus the boundaries of the aggregated structures vary in time or, equivalently, with convection downstream, but in a predictable fashion. This may have implications for the eddy shapes used in classical AEM formulations, in which dynamic evolution is not present. It should also lead to some insight into time-evolution of uniform momentum zones (Figure 1(h)).

III. REQUIREMENTS FOR SELF-SUSTAINING SELF-SIMILARITY

Besides the aspects of temporal evolution elucidated by the linear analysis above, insight into nonlinear interactions and therefore the mechanisms by which turbulence self-sustains can also be obtained, an analytical analog of the numerical solutions cited earlier, derived from the NSE and the mean profile. A direct connection between the AEM and the self-sustaining minimal solutions in the log region in the literature has been previously alluded to [3], but not demonstrated.

The linearity of the velocity decomposition in the resolvent framework means that hierarchies can be linearly superposed, with the nonlinear interactions determining the wavenumbers and weights which are required for consistency with the nonlinear NSE. It is simple to show [21, 22] that the quadratic interaction between hierarchies is self-similar, meaning that if modes on a set of three hierarchies are triadically consistent (resonant) at one location in the overlap region, they will also be resonant at other wall-normal heights on the same hierarchies. Further, self-similar interaction coefficients, $\mathcal{M}_{lij}$, can be defined for the excitation of hierarchy l by hierarchies i, j over all y heights where self-similarity is observed. These depend only on separation of the y-location of interest and the reference height, y_r (or, equivalently, c and c_r) such that:

$$\chi_l^*(\boldsymbol{\lambda}, c) \;=\; \mathrm{e}^{2.5\kappa(c_r - c)} \sum_{i,j=1}^{N} \iint \mathcal{M}_{lij}(\boldsymbol{\lambda}_r, \boldsymbol{\lambda}_r', c' - c)\, \chi_i(\boldsymbol{\lambda}', c')\, \chi_j^*(\boldsymbol{\lambda}'', c'')\; \mathrm{d}\ln\boldsymbol{\lambda}_r'\, \mathrm{d}c', \tag{13}$$

i.e., from Equation 7,

$$\mathcal{N}_{lij}(\boldsymbol{\lambda}, c, \boldsymbol{\lambda}', c') = \mathrm{e}^{2.5\kappa(c_r - c)} \mathcal{M}_{lij}(\boldsymbol{\lambda}_r, \boldsymbol{\lambda}_r', c' - c). \tag{14}$$

Thus, for some range of spatial and temporal scales, it is possible that interactions between hierarchies at one height are replicated in a scaled, self-similar way at other locations in the overlap region, provided that the weights, $\chi(\boldsymbol{\lambda}, c)$, are also self-similar and that the influence of modes that are not self-similar is minimal.

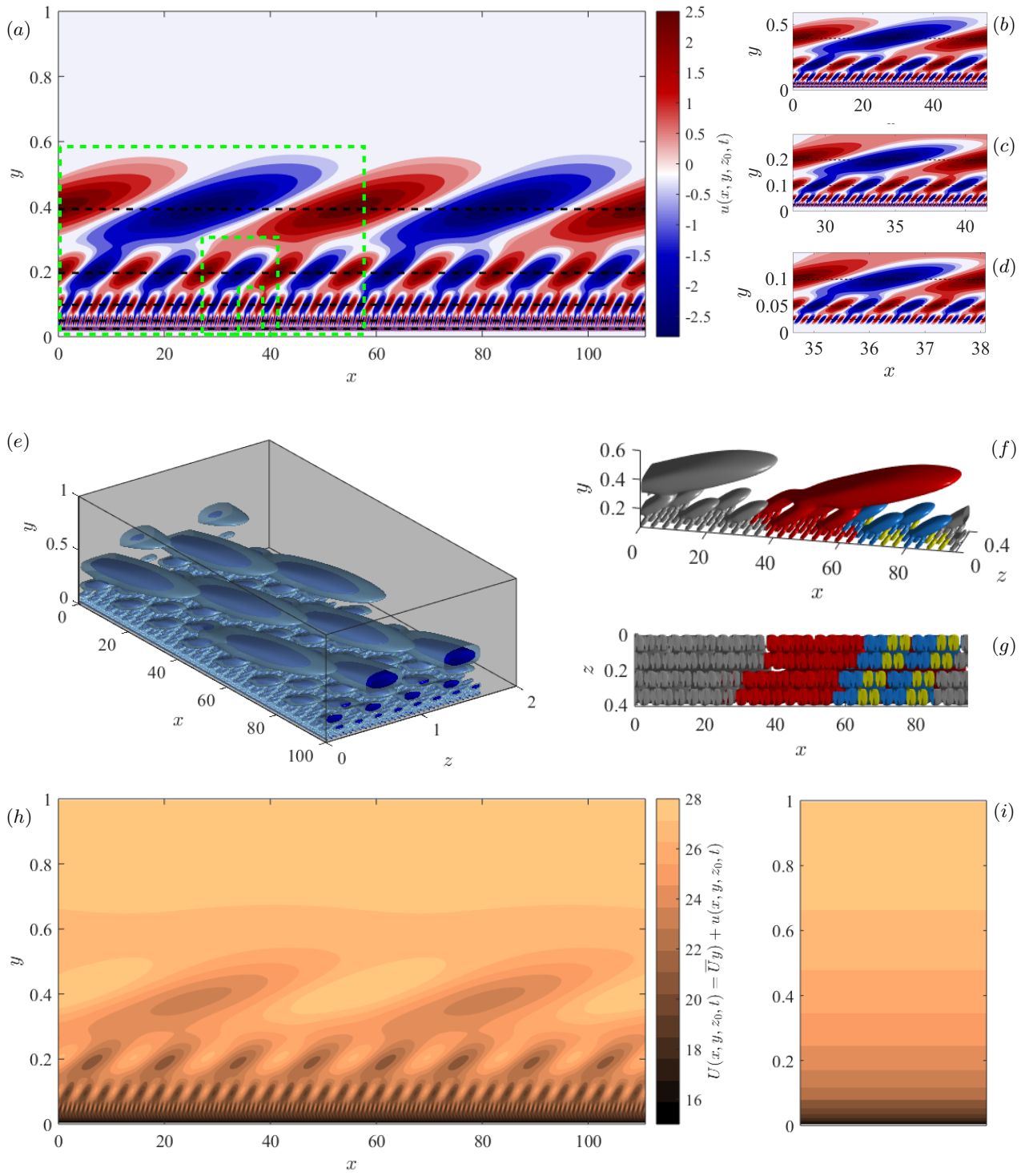

FIG. 1. Self-similar structure on a resolvent hierarchy in channel flow at $Re_\tau = 15,000$: $\mathcal{S}(\boldsymbol{\lambda}_r)$, with $(\boldsymbol{\lambda}_r, c_r) = (\boldsymbol{\lambda}_5, c_5) = (29, 123, U(y_{c5}))$ defined as the largest scale on the hierarchy. $y_{c1} = 0.4$, $y_m = A^{1-m} y_1$ and $|A| = 2$. Here all modes have the same peak amplitude, $0.1U(1)$. (a)-(d): Isocontours of instantaneous streamwise fluctuation on an (x, y) plane, $u(x, y, z_0 = 0, t_0)$ for $z = 0$ symmetric modes. y_{cm} marked by black dashed lines and green dashed boxes in (a) identify the regions extracted in (b)-(d). (e) Three-dimensional isosurfaces of negative $u(x, y, z, t_0)$ for $z = 0$ antisymmetric modes. (f)-(g) Aggregated structures in a single period of the largest scale, color-coded by the appropriate scaling height, y_{cm}. Red, blue and yellow: m=1,2,3, respectively. (h)Instantaneous streamwise velocity on an (x, y) plane, $U(x, y, z_0, t_0)$, for the fluctuations in (a)-(d) added to the turbulent mean shown in (i). Note the aspect ratios in this figure.

Further, the Reynolds-Orr equation for the energy budget associated with a single mode in a hierarchy [21] gives

$$E_P(\boldsymbol{\lambda}, c) - E_D(\boldsymbol{\lambda}, c) = E_T(\boldsymbol{\lambda}, c) \tag{15}$$

with

$$E_P(\boldsymbol{\lambda}, c) = -\left(\frac{2\pi}{\lambda_x}\right)^2 \left(\frac{2\pi}{\lambda_z}\right) \int_0^2 \mathrm{Re}\left\{U_y(y)\hat{u}(y, \boldsymbol{\lambda}, c)^* \hat{v}(y, \boldsymbol{\lambda}, c)\right\} \mathrm{d}y \tag{16}$$

$$E_D(\boldsymbol{\lambda}, c) = \frac{1}{Re_\tau}\left(\frac{2\pi}{\lambda_x}\right)^2 \left(\frac{2\pi}{\lambda_z}\right) \int_0^2 (\hat{\mathbf{u}}_y(y, \boldsymbol{\lambda}, c)^* \hat{\mathbf{u}}_y(y, \boldsymbol{\lambda}, c) + k^2 \hat{\mathbf{u}}(y, \boldsymbol{\lambda}, c)^* \hat{\mathbf{u}}(y, \boldsymbol{\lambda}, c) \mathrm{d}y \tag{17}$$

$$E_T(\boldsymbol{\lambda}, c) = -\left(\frac{2\pi}{\lambda_x}\right)^2 \left(\frac{2\pi}{\lambda_z}\right) \int_0^2 \mathrm{Re}\left\{\hat{\mathbf{u}}(y, \boldsymbol{\lambda}, c)\hat{\mathbf{f}}(y, \boldsymbol{\lambda}, c)\right\} \mathrm{d}y. \tag{18}$$

On a self-similar hierarchy with self-similar weights, the mode scaling implies self-similarity of $E_P(\boldsymbol{\lambda}, c)$ and $E_D(\boldsymbol{\lambda}, c)$, while $E_T(\boldsymbol{\lambda}, c)$ must also be self-similar if the forcing, $\hat{\mathbf{f}}(y, \boldsymbol{\lambda}, c)$, arises from the interactions between continuous hierarchies (Equations 5, 11, 14, see [21] for further discussion).

If the real velocity field can be modeled as an integral over hierarchies, $\mathcal{S}(\boldsymbol{\lambda}_r)$, then the scaling results above admit the somewhat remarkable possibility of determining from the equations of motion velocity fields, nonlinear interactions and energy budgets which are all self-similar and scale with distance from the wall, and closing the NSE using resolvent modes.

IV. SUMMARY AND CONCLUSIONS

Geometric self-similarity of the linear Navier-Stokes operator for turbulent flow has been observed by several authors, however the self-similar scaling (in spectral space) was in disagreement with the full distance-from-the-wall scaling of Townsend and the AEM. It has been shown here that this apparent conflict can be resolved by making an "apples-to-apples" structural comparison, following the common AEM representation of a geometric progression (rather than a continuous distribution) of eddy sizes. The aggregated structures associated with a geometrically self-similar resolvent hierarchy shown in Figure 1 obey the attached eddy scaling and reveal a stricter spatial exclusion than previously posited through the AEM. However these aggregations exist relative to the turbulent mean profile, which is assumed (equally, acts as a constraint) in the resolvent framework, whereas attached eddies are superposed on a uniform flow.

The resolvent formulation also reveals spatio-temporal information, i.e. dynamics, associated with the self-similar resolvent hierarchies. Members of a hierarchy move with different convection velocities, meaning that while the aggregations are self-similar at a given instant, their boundaries evolve in time, in a self-similar way, with further implications for the direct comparison with the AEM. The results of [21] and [22] concerning self-similarity of the nonlinear interactions between resolvent hierarchies reveal the possibility of self-sustaining assemblies of hierarchies, with likely connection to the self-similar, self-sustaining solutions obtained in minimal unit simulations in the logarithmic layer.

The connection between the velocity response modes which are naturally most amplified in the equations of motion, parameterized in spectral space, and empirical physical space reasonings going back to Townsend seems to hold promise both for improved modeling in both domains. We have focused on the first resolvent modes herein, but the approach can be extended to consider higher rank resolvent approximations and to include the separate consideration of Orr-Sommerfield and Squire contributions to the wall-normal vorticity, which was identified by [27] as an important step in obtaining an efficient basis to represent real flows. The weights, $\chi_j(\boldsymbol{\lambda}, c)$, hold the key to nonlinear closure of the resolvent framework; the work herein suggests that analytical progress to complement data-driven resolvent approaches, e.g. [20, 28, 29], may be made. Connections between the resolvent results, the AEM, self-similar minimal unit and exact coherent solutions, and the mean flow similarity of the MMB are the topic of ongoing work.

ACKNOWLEDGEMENTS

The support of ONR through grant N00014-17-1-3022 is gratefully acknowledged.

[1] A. A. Townsend. The structure of the turbulent boundary layer. *Math. Proc. Camb. Philos. Soc.*, 47:375–395, 1951.

[2] A. A. Townsend. *The Structure of Turbulent Shear Flow*. Cambridge University Press, Cambridge, UK, 1976.

[3] I. Marusic and J. P. Monty. Attached eddy model of wall turbulence. *Annu. Rev. Fluid Mech.*, 51:49–74, 2019.

[4] I. Marusic, J. P. Monty, M. Hultmark, and A. J. Smits. On the logarithmic region in wall turbulence. *J. Fluid Mech.*, 716:R3, 1–11, 2012.

[5] W. J. Baars, N. Hutchins, and I. Marusic. Self-similarity of wall-attached turbulence in boundary layers. *J. Fluid Mech.*, 823(R2), 2017.

[6] Y. Hwang. Statistical structure of self-sustaining attached eddies in turbulent channel flow. *J. Fluid Mech.*, 767:254–289, 2015.

[7] L. Agostini and M. Leschziner. Spectral analysis of near-wall turbulence in channel flow at $Re_\tau = 4200$ with emphasis on the attached-eddy hypothesis. *Phys. Rev. Fluids*, 2(014603), 2017.

[8] C.M. de Silva, N. Hutchins, and I. Marusic. Uniform momentum zones in turbulent boundary layers. *J. Fluid Mech.*, 786:309–331, 2016.

[9] C. M. de Silva, J. D. Woodcock, N. Hutchins, and I. Marusic. Influence of spatial exclusion on the statistical behavior of attached eddies. *Phys. Rev. Fluids*, 1(022401), 2016.

[10] A. E. Perry and I. Marusic. A wall-wake model for the turbulence structure of boundary layers. Part 1. Extension of the attached eddy hypothesis. *J. Fluid Mech.*, 298:361–388, 1995.

[11] O. Flores and J. Jiménez. Hierarchy of minimal flow units in the logarithmic layer. *Phys. Fluids*, 22(071704), 2010.

[12] Y. Hwang and Y. Bengana. Self-sustaining process of minimal attached eddies in turbulent channel flow. *J. Fluid Mech.*, 795:708–338, 2016.

[13] Q. Yang, A. P. Willis, and Y. Hwang. Exact coherent states of attached eddies in channel flow. *J. Fluid Mech.*, 862:1029–1059, 2019.

[14] J. Jiménez and P. Moin. The minimal flow unit in near-wall turbulence. *J. Fluid Mech.*, 225:213–240, 1991.

[15] J. C. Klewicki, J. Philip, I. Marusic, K. Chauhan, and C. Morrill-Winter. Self-similarity in the inertial region of wall turbulence. *Phys. Rev. E*, 90:823–839, 2014.

[16] J. C. del Álamo and J. Jiménez. Linear energy amplification in turbulent channels. *J. Fluid Mech.*, 559:205–213, 2006.

[17] Y. Hwang and C. Cossu. Linear non-normal energy amplification of harmonic and stochastic forcing in the turbulent channel flow. *J. Fluid Mech.*, 664:51–73, 2010.

[18] B. J. McKeon and A. S. Sharma. A critical layer model for turbulent pipe flow. *J. Fluid Mech.*, 658:336–382, 2010.

[19] B. J. McKeon, A. S. Sharma, and I. Jacobi. Experimental manipulation of wall turbulence: a systems approach. *Phys. Fluids*, 25(031301), 2013.

[20] R. Moarref, A. S. Sharma, J. A. Tropp, and B. J. McKeon. Model-based scaling and prediction of the streamwise energy intensity in high-Reynolds number turbulent channels. *J. Fluid Mech.*, 734:275–316, 2013.

[21] R. Moarref, A. S. Sharma, J. A. Tropp, and B. J. McKeon. A foundation for analytical developments in the logarithmic region of turbulent channels. *ArXiv*, (1409.6047), 2014.

[22] A. S. Sharma, R. Moarref, and B. J. McKeon. Scaling and interaction of self-similar modes in models of high-Reynolds number wall turbulence. *Phil. Trans. Royal Soc. A*, 375(2089)(20160089), 2016.

[23] S. B. Vadarevu, S. Symon, S. J. Illingworth, and I. Marusic. Coherent structures in the linearized impulse response of turbulent channel flow. *J. Fluid Mech.*, 863:1190–1203, 2019.

[24] B. J. McKeon. The engine behind (wall) turbulence: perspectives on scale interactions. *J. Fluid Mech.*, 817:P1, 2017.

[25] I. Tobasco and C. Doering. Optimal wall-to-wall transport by incompressible flows. *Phys. Rev. Letters*, 118(264502), 2017.

[26] T. Saxton-Fox and B. J. McKeon. Coherent structures, uniform momentum zone and the streamwise energy spectrum in wall-bounded turblent flows. *J. Fluid Mech.*, 826(R6), 2017.

[27] K. Rosenberg and B. J. McKeon. Efficient representation of exact coherent states of the Navier-Stokes equations using resolvent analysis. *Fluid Dyn. Res.*, 51(011401), 2019.

[28] S. J. Illingworth, J. P. Monty, and I. Marusic. Estimating large-scale structures in wall turbulence using linear models. *J. Fluid Mech.*, 842:146–162, 2018.

[29] A. Towne, Lozano-Durán, and X. Yang. Resolvent-based estimation of space-time flow statistics. *ArXiv*, (1901-07478), 2019.